ChemComm

Optimizing Pulsed Laser Deposition of Crystalline $BiVO_4$ Thin Film on Yttrium-stabilized Zirconia (110) Substrates

Journal:	*ChemComm*
Manuscript ID	CC-COM-07-2024-003301.R1
Article Type:	Communication

ChemComm

COMMUNICATION

Optimizing Pulsed Laser Deposition of Crystalline BiVO4 Thin Film on Yttrium-stabilized Zirconia (110) Substrates

Received 00th January 20xx,

Zhaoyi Xi[a,b], Chenyu Zhou[a], Kim Kisslinger[a], and Mingzhao Liu[a*]

Different conditions are explored to understand their effects on the pulsed laser deposition of $BiVO_4$ water splitting photoanodes, over YSZ (110) substrates. A two-step deposition (TSD) method can independently tune nucleation and bulk film growth, leading to the formation of phase pure, crystalline $BiVO_4$ film with optimized water splitting activities.

Pulsed laser deposition (PLD) is a promising thin film deposition method, which offers an alternative and novel way for controllable deposition of all kinds of oxides, nitrides, carbides, and polymers layers over substrates[1-3]. PLD is a physical vapor deposition method, in which a high-power pulsed laser, usually an excimer laser (e.g., KrF, ArF, or XeCl), ablates a ceramic or metallic target in a high vacuum chamber. Under the focused laser spot, the target is locally ionized to form a plasma that contains the depositing flux, i.e., the laser plume. A thin film of the target material is then deposited on the substrate from the laser plume.[4-6] PLD has a few notable characters, such as stoichiometric transfer from laser target, great flexibility in the selection of materials, and the capability of reactive deposition in ambient gases.[7, 8] During the past few decades, PLD has been heavily involved for depositing thin film materials of technological relevance[9, 10]. For many of such applications, the deposition condition of PLD must be carefully adjusted to optimize the desired material properties[9, 10].

One emerging application of PLD during the past decade is the fabrication of high-quality thin film materials for solar energy conversion, including photovoltaic cells, perovskite solar cells, organic photovoltaics, and photoelectrochemical cells[11-14]. Light harvesting based on photocatalytic generation of chemical fuels, or artificial photosynthesis, has long been sought as a promising renewable solar energy technology[15-17]. Solar water splitting in a photoelectrochemical cell, in which water is split into hydrogen (H_2) and oxygen (O_2), has been widely studied as a realization of artificial photosynthesis[18, 19]. Out of the wide range of materials studied for water splitting photoelectrode, bismuth vanadate ($BiVO_4$, BVO) has been recognized as one of the top candidates, for its visible light optical gap (2.4 – 2.6 eV), suitable band alignment with respect to water redox reactions, decent chemical stability, and low toxicity[20-22]. PLD has been deployed as a very reliable method to fabricate BVO thin films. For example, our group have extensively studied the epitaxial growth of BVO films on (001)-oriented single crystalline yttrium-stabilized cubic zirconia (YSZ) substrates and their application as solar water splitting photoanodes.[20, 23-25] More recently, it was shown that PLD BVO photoanode can be used for photoelectrochemical chlorine generation reaction (ClER) as well[23]. However, to date, all BVO photoanodes were fabricated over YSZ (001) substrate due to existence of a straightforward epitaxial relation. There is relatively little knowledge on the PLD growth behavior of BVO on other substrate, or on other facets of the YSZ substrate.

In this work, we report a systematic study on optimizing PLD growth condition to fabricate crystalline BVO thin films over YSZ substrates cut in the (110) orientation. The study indicates that the optimized PLD condition departs significantly away from the recipe previously optimized for growth over YSZ (001). In particular, we find that a two-step deposition (TSD) method, in which different growth conditions are applied during the nucleation phase and the domain growth phase, enables the formation of dense, flat, and crystalline BVO film with quality similar as the conventional one-step growth over YSZ (001). We further find that the BVO thin film morphology and domain structure can be readily tuned by deposition conditions such as deposition temperature and background oxygen pressure, which subsequently leaves substantial impact on their PEC water splitting activities.

$BiVO_4$ (BVO) thin film photoanodes are fabricated over single crystalline, (110)-oriented yttrium-stabilized zirconia substrates (YSZ (110)), by PLD. Prior to the deposition of BVO, a buffer layer of indium tin oxide (ITO, cubic, space group $Ia\bar{3}$) is first deposited by PLD in high vacuum, as a transparent conductive back contact. In our earlier work, the PLD fabrication of BVO photoanode over YSZ (001) had been optimized with a substrate temperature of 675°C , an oxygen pressure of 10 mTorr, and a laser repetition rate of 20 Hz.[20, 23, 24] However, once switched to the YSZ (110) substrates, this deposition condition can no longer produce the same dense and flat film morphology, or the uniform crystalline orientation. As shown by its scanning electron microscopy (SEM) image, when adopting

[a] Center for Functional Nanomaterials, Brookhaven National Laboratory, Upton, New York 11973, United States *Email: mzliu@bnl.gov
[b] Department of Materials Science and Chemical Engineering, Stony Brook University, Stony Brook, New York 11794, United States
† Footnotes relating to the title and/or authors should appear here.
Supplementary Information available:

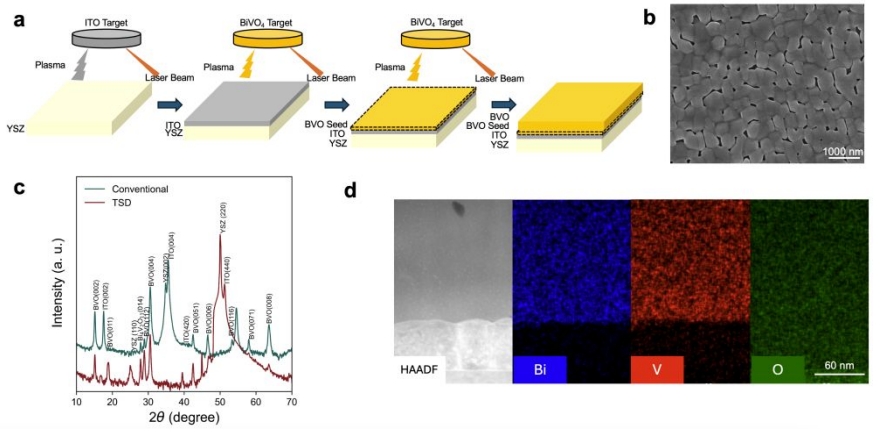

Figure 1. (a) Schematics of the two-step-deposition (TSD) method for fabricating BVO thin film photoanode on YSZ (110) substrate. Prior to the TSD growth of BVO thin film, an ITO layer is first deposited as transparent back contact. (b) An SEM image of TSD BVO thin film over YSZ (110). (c) The XRD patterns of BVO thin films deposited over YSZ (001) with the conventional one-step method and over YSZ (110) with the TSD method. (d) HAADF-STEM image showing a cross-sectional view of the $BiVO_4$/ITO/YSZ (110) photoanode, with simultaneously collected EDX elemental mapping for the spatial distribution of Bi, V and O.

the conventional condition for deposition over YSZ (110), the BVO film appears rough with wide gaps developed between BVO columnar domains (ESI Figure S1b).

Various modifications to the conventional condition are made to accommodate the YSZ (110) substrates. While deposition temperature is a common tunning knob for thin film growth by PLD, we find that neither lowering nor increasing the substrate temperature from 675°C leads to desirable improvement (ESI Figure S1). At a lower substrate temperature of 650°C, although the film appears overall smoother under SEM, X-ray diffraction (XRD) reveals the formation of $Bi_4V_2O_{11}$ in addition to the desired monoclinic $BiVO_4$ phase (ESI Figure S2). On the other hand, at higher deposition temperatures (700°C and 725°C, ESI Figure S1c and S1d), the BVO thin films become rougher with even wider gaps developed between grains. Wider gaps between domains will negatively impact charge transport within BVO film and introduce more recombination centers. For these reasons, we will keep the substrate temperature at 675°C throughout the rest of this study.

By reducing the laser repetition rate from 20 Hz to 1 Hz and thereby drastically decreasing the growth rate, large BVO domains are formed in dense packing, despite that the film remains very rough (ESI, Figure S3). This may be attributed to the slower nucleation process, which leads to sparse nucleation and prevents the formation of a uniform growth front. To overcome this problem, we develop a two-step deposition (TSD) method (Figure 1a), in which a 20-nm-thick "seeding" layer of BVO is first deposited at a higher laser repetition rate (typically 5 Hz), to help achieve the desired uniform nucleation. In the second step, the bulk of BVO film is grown to a nominal thickness of 150 nm, at a lower laser repetition rate (typically 1 Hz) to achieve the desired dense packing of domains. Through the TSD method, BVO thin film deposited over YSZ (110) achieves a dense and flat grain structure (Figure 1b) that has comparable quality and surface morphology as BVO deposited over YSZ (001) using the conventional, one step method[23]. The BVO coverage reaches 98.7%, with uniform, circular domains that are about 450 nm in diameter. On the contrary, BVO films deposited through the conventional one-step method generally have coverage below 90%, with elongated, irregular domains, due to the presence of extensive gaps between domains (ESI Figure S1). A vertical cross-sectional specimen of TSD BVO thin film is studied by scanning transmission electron microscopy (STEM), using high-angle annular dark field (HAADF) imaging and concurrent energy-dispersive X-ray spectroscopy (EDX) mapping. The study confirms the chemical homogeneity throughout the BVO film, with uniform distribution of elements Bi, V, and O (Figure 1d). Details of the TSD method are discussed in the *ESI*.

X-ray diffraction (XRD) study on BVO grown over YSZ (110) confirms a crystal structure of monoclinic scheelite (space group I2/b, PDF no. 14-0688). The diffraction pattern appears nearly identical as BVO grown over YSZ (001), with clear dominance by *c*-plane (00*l*) diffraction peaks of BVO (Figure 1c). Due to the strong diffraction peaks from the YSZ substrate, the diffraction intensities are presented in logarithmic scale. We must note that, in the case of BVO grown over YSZ (001), the preferred (001) orientation of BVO domains is stabilized by the epitaxial relationships between the facets of BVO [001], ITO [001], and YSZ [001]. For the deposition over YSZ (110), although the ITO buffer layer grows epitaxially along the (110) orientation, as confirmed by its (440) diffraction peak at 50.136° (Figure 1c and ESI Figure S5), the BVO domains remain in the preferred (001) orientation despite the lack of an apparent epitaxial relationship with the underlaying substrate. In this case, the (001) orientation must instead be stabilized by surface energy, which may explain why we must drastically change the deposition condition from the one optimized for YSZ (001).

The BVO thin film morphology and crystalline structure are robust once it is formed at 675°C. Regardless of the rates of

post-growth cooling, which are respectively set at 5, 10, 20, and 25°C min^{-1}, the TSD method produces BVO thin films that appear flat and uniform, with a dense columnar microstructure (ESI Figure S4). BVO thin films fabricated with different post-growth cooling rates produce nearly identical XRD patterns, which confirms that the cooling rate has negligible influence on the thin films growth (ESI Figure S6).

Besides the deposition temperature, another key tuning knob for PLD thin film growth is the background pressure. While the one-step, conventional growth of BVO on YSZ (001) are typically conducted with an oxygen pressure (p_{O_2}) of 20 mTorr[26], we find that the TSD method for BVO growth on YSZ (110) is optimized with a lower p_{O_2}. For this demonstration, the growth on YSZ (110) is studied with a wide range of p_{O_2}, varying from 10 mTorr to 60 mTorr, under otherwise identical conditions. The impact of p_{O_2} on the morphology of BVO thin film is clearly visualized from their top-view SEM images (Figure 2a~c and ESI Figure S7). The BVO thin film deposited with $p_{O_2} = 10$ mTorr is flat and features densely packed domains separated by clear boundaries. While increasing p_{O_2} to 15 mTorr only brings subtle change to surface morphology (ESI Figure S7a), a clear difference is observed when p_{O_2} reaches 20 mTorr, at which point the BVO domains appear more faceted and less flat, despite remaining densely packed (Figure 2b). Toward even higher p_{O_2}, the BVO film becomes more grainy, with incrementally smaller domains (Figure 2c and ESI Figures S7b-c). For instance, the BVO domain size from 40 mTorr deposition is only about half as the one from 20 mTorr deposition. Nevertheless, BVO domains remain densely packed

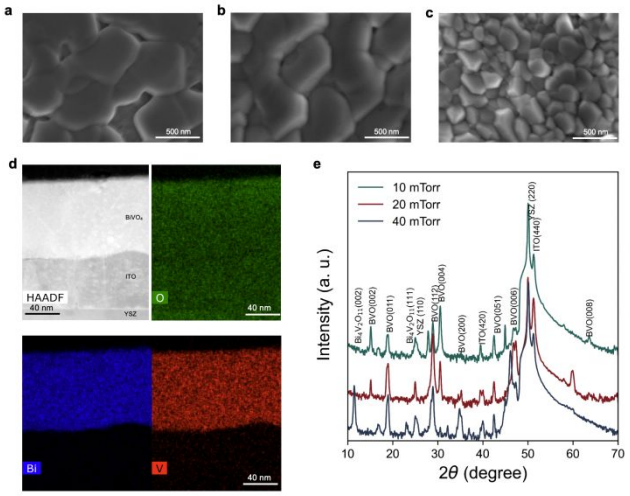

Figure 2. SEM images of BVO/ITO/YSZ (110) photoanodes fabricated by the TSD method, with oxygen pressure during deposition set at (a) 10 mTorr, (b) 20 mTorr, (c) 40 mTorr. (d) HAADF-STEM image reveals the crystalline lattice of BVO; (d) HAADF-STEM image showing a cross-sectional view of a BVO/ITO/YSZ (110) photoanode fabricated with $p_{O_2} = 40$ mTorr, with EDX elemental mapping for the spatial distribution of Bi, V and O, collected simultaneously with the HAADF-STEM image. (e) XRD patterns of BVO/ITO/YSZ (110) photoanodes fabricated by the TSD method, with different oxygen pressure during deposition.

up to the highest p_{O_2} tested (60 mTorr), proving the robustness of the TSD method.

STEM and EDX studies on a BVO film deposited under higher p_{O_2} (40 mTorr) (Figure 2d) suggest that the film remains chemically homogeneous, with uniform elemental distribution of Bi, V, and O. On the other hand, from cross-sectional SEM studies (ESI Figure S8), we find that the film thickness decreases monotonically against increasing p_{O_2}. The BVO film thicknesses are 170, 124, and 110 nm, for samples respectively grown under 10, 20, and 40 mTorr of oxygen pressure. The trend is due to the backscattering of laser plume by background gas molecules, which decreases the deposition rate. Accordingly, BVO film deposited at the lowest p_{O_2} (10 mTorr) achieves the highest optical density in its UV-Vis absorption spectra, with lower optical absorbance observed for higher p_{O_2} samples (Figure 3b). Tauc plots find that the optical gap is 2.60 eV for BVO film deposited under 10 and 20 mTorr of p_{O_2}, but red-shifts slightly to 2.54 eV for higher p_{O_2} samples (ESI Figure S9). Although XRD confirms that the BVO thin films fabricated under different values of p_{O_2} are all dominated by the monoclinic $BiVO_4$ phase, there is a minor presence of the impurity $Bi_4V_2O_{11}$ phase for BVO thin films deposited with $p_{O_2} \geq 30$ mTorr (Figure 2e and ESI Figure S10). The formation of the bismuth-rich $Bi_4V_2O_{11}$ phase is possibly due to the more effective backscattering of V atoms by the oxygen molecules, since V has a much lower atomic mass than Bi (50.94 vs. 208.98). In addition, we note the emergence of the $Bi_4V_2O_{11}$ impurity phase is accompanied by the disappearance of the set of $BiVO_4$ (00*l*) diffractions peaks, which demonstrates the impact of the impurity phase on the grain structure. It was reported that $Bi_4V_2O_{11}$ has a narrower band gap than $BiVO_4$, which explains the optical gap red-shift observed for the higher p_{O_2} BVO thin films.[27]

The impact of p_{O_2} on the water splitting activities of BVO thin films is studied by photoelectrochemistry (PEC) measurements (Figure 3a). The measurements are conducted in a pH = 7 phosphate buffer, with sodium sulfite (Na_2SO_3) added as the hole scavenger. The BVO thin films deposited under different p_{O_2} are used as the working electrodes and are illuminated by simulated AM 1.5G solar simulation, from the back side, i.e., through the YSZ substrate and the ITO back contact. The illumination direction is chosen to compensate the low electron mobility of BVO, which is due to the formation of small polarons.[26] For BVO photoanode deposited under $p_{O_2} = 10$ mTorr, a photocurrent density of 1.85 mA cm^{-2} is observed at 1.23 V_{RHE}, the thermodynamical potential for oxygen evolving. The photocurrent remains stable for at least 180 min (ESI Figure S11). For the one deposited under $p_{O_2} = 20$ mTorr, the photocurrent density at 1.23 V_{RHE} drops slightly to 1.65 mA cm^{-2}. As p_{O_2} increases further, the photocurrent density at 1.23 V_{RHE} drops more dramatically, to 0.5 mA cm^{-2} for the 40 mTorr sample, and finally to 0.3 mA cm^{-2} for the 60 mTorr sample, with significant anodic shift of the photocurrent onset potential.

The decrease of photocurrent can certainly be partially attributed to the finding that higher p_{O_2} leads to thinner BVO film, which has lower optical density and generates less charge carriers. However, it must be noticed that the photocurrent drops much faster than the decrease of film thickness. For instance, with p_{O_2}increased from 10 mTorr to 40 mTorr, the

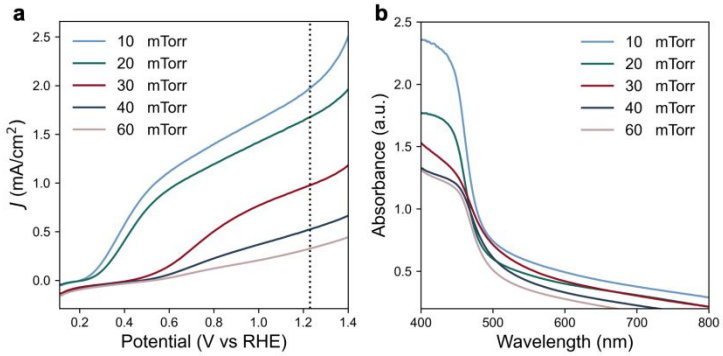

Figure 3. (a) Photocurrent density versus potential curves of BVO/ITO/YSZ (110) photoanodes fabricated under different oxygen pressures from 10 to 60 mTorr, under simulated AM 1.5G solar radiation. The electrolyte is a sulfite phosphate buffer solution buffered to pH = 7; (b) UV-Vis spectra of the same group of sample.

BVO layer thickness decreases from 170 nm to 110 nm, but the photocurrent density drops sharply from 1.85 mA cm^{-2} to 0.3 mA cm^{-2}. In addition, as shown in ESI Figure S9, even the thinnest BVO film, deposited with $p_{O_2} = 60$ mTorr, achieves an optical density over 1.2 for excitation above its band gap (λ < 480 nm), which corresponds to over 93% absorption of incident light. Therefore, the extra photons that are absorbed by a thicker BVO film can only increase the photocurrent by at most a few percent. This suggests that an additional mechanism must be responsible for the drastic decrease of photocurrent. Indeed, we note that samples fabricated with $p_{O_2} \geq 30$ mTorr all contain small amount of the $Bi_4V_2O_{11}$ impurity, which may act as a charge trap for charge carriers generated in $BiVO_4$ and deteriorates the PEC activity. Electrochemical impedance spectroscopy (EIS) measurements reveal that the interfacial charge transfer resistance (R_{ct}) drastically increases for samples grown under higher p_{O_2}(ESI Figure S12, Table S1). This suggests a more significant charge recombination and is consistent with the role of $Bi_4V_2O_{11}$ impurity as a charge trap. The anodic shift of photocurrent onset potential can also be attributed to charge trapping by the $Bi_4V_2O_{11}$ impurity.

In summary, we find that high quality, crystalline $BiVO_4$ (BVO) thin films can be grown over YSZ (110) substrates utilizing a two-step deposition (TSD) method, which offers additional degree of freedom to separately optimize the nucleation and domain growth processes. By adjusting deposition parameters, including substrate temperature and laser repetition rate, we manage to fabricate BVO thin film on YSZ (110) with quality comparable to those deposited on YSZ (001) via the conventional one-step method. The background oxygen pressure is also found to have significant impact on the film quality, with lower oxygen pressure (10 mTorr) being more favorable for the formation of dense, flat, and phase pure $BiVO_4$ film that also shows the highest PEC water splitting activity. At higher oxygen pressures, an impurity $Bi_4V_2O_{11}$ phase emerges and significantly suppresses the water splitting activity. Overall, this research demonstrates the versality of the two-step PLD method in optimizing the growth of crystalline thin film materials and offers a promising strategy that is generally applicable for a wide range of complex metal oxide thin films.

This research used Materials Synthesis & Characterization and Electron Microscopy facilities of the Center for Functional Nanomaterials (CFN), which is a U.S. Department of Energy Office of Science User Facility, at Brookhaven National Laboratory under Contract No. DE-SC0012704.

Data availability

The data supporting this article has been included as part of ESI.

Notes and references

(1) Chrisey, D. B et al. *Handbook of Laser Technology and Applications* **2003**.
(2) Christen, H. M et al. *J Phys Condens Matter* **2008**, *20* (26), 264005.
(3) Krebs, H.-U. et al. *Advances in Solid State Physics*, Kramer, B. Ed.; Springer Berlin Heidelberg, 2003; pp 505-18.
(4) Aziz, M. J. *Appl. Phys. A* **2008**, *93* (3), 579-87.
(5) Chrisey, D. B et al. Pulsed Laser Deposition of Thin Films. **1994**.
(6) Hubler, G. K. *MRS Bulletin* **1992**, *17* (2), 26-9.
(7) Lowndes, D. H et al. *Science* **1996**, *273* (5277), 898-903.
(8) Tayebi, M. et al. *Renew. Sustain. Energy Rev.* **2019**, *111*, 332-43.
(9) Moriya, K. et al. *Jpn. J. Appl. Phys.* **2007**, *46* (9R), 5780.
(10) Gupta, R. K. et al. *Physica E Low Dimens. Syst. Nanostruct* **2009**, *41* (4), 617-20.
(11) Bergqvist, J. et al. *Prog Photovolt* **2016**, *24* (8), 1096-108.
(12) Park, J. H. et al. *Adv. Mater.* **2015**, *27* (27), 4013-9.
(13) Schubert, S. et al. *Adv. Funct. Mater.* **2015**, *25* (27), 4321-7.
(14) Fàbrega, C. et al. *Appl. Catal. B* **2016**, *189*, 133-40.
(15) Fujishima, A. et al. *Nature* **1972**, *238* (5358), 37-8.
(16) Nozik, A. J. *Annu. Rev. Phys. Chem.* **1978**, *29* (1), 189-222.
(17) Walter, M. G. et al. *Chem. Rev.* **2010**, *110* (11), 6446-73.
(18) Andreiadis, E. S. et al. *Photochem. Photobiol.* **2011**, *87*, 946-64.
(19) Grätzel, M. *Nature* **2001**, *414* (6861), 338-44.
(20) Zhou, C. et al. *ACS Appl. Mater. Interfaces* **2021**, *13* (51), 61227-36.
(21) Lee, D. et al. *Nat. Energy* **2021**, *6* (3), 287-94.
(22) Hilbrands, A. M. et al. *J. Am. Chem. Soc.* **2023**, *145* (43), 23639-50.
(23) Xi, Z. et al. *ACS Appl. Mater. Interfaces* **2023**, *15* (42), 49281-8.
(24) Zhou, C. et al. *Chem. Mater.* **2020**, *32* (15), 6401-9.
(25) Zhang, W. et al. *J. Phys. Chem. C* **2019**, *123* (34), 20730-6.
(26) Kristmannsdóttir, H. et al. *Geothermics* **2003**, *32* (4), 451-61.
(27) dos Santos, W. S. et al. *Sci. Rep.* **2016**, *6* (1), 31406.

Data Availability Statement

The data supporting this article have been included as part of the Supplementary Information.

Dr. Mingzhao Liu
Senior Scientist
Center for Functional Nanomaterials
Brookhaven National Laboratory
Email: mzliu@bnl.gov